NANO · MICRO small
www.small-journal.com

Chalcogenide Photonic Crystals Fabricated by Soft Imprint-Assisted Photodoping of Silver

Le Wei, Jingjing Qian, Liang Dong, and Meng Lu**

This work presents a low-cost, large-scale nanofabrication approach that combines imprint lithography and silver doping (IL-SD) to pattern chalcogenide glass (ChG) films for realizing IR devices. The IL-SD method involves controled photodoping of silver (Ag) atoms into ChG films and selective removing of undoped ChG. For photodoping of Ag, an Ag-coated elastomer stamp is brought in contact with the ChG film and exposed to ultraviolet light, and subsequently, the Ag atoms are photo-dissolved into the ChG film following the nanopatterns on the elastomer stamp. Due to the high wet-etching selectivity of the undoped ChG to Ag-doped one, the ChG film can be precisely patterned with a spatial resolution on the order of a few tens of nanometers. Also, by controling the lateral diffusion of Ag atoms during ultraviolet exposure, it is possible to adjust the size of the final patterns formed in the ChG film. As an application demonstration of the IL-SD process, the As_2S_3-based near-infrared photonic crystals (PhCs) in the wavelength range and flexible midinfrared PhCs are formed, and their optical resonances are investigated. The IL-SD process enables the low-cost fabrication of ChG nanostructures on different substrate materials and gives a great promise to realize various IR devices.

1. Introduction

Featured with a low material loss in the IR wavelength range, chalcogenide glass (ChG) materials, such as As_2S_3, GeSbTe, and AgInSbTe, have attracted increasing attention for a variety of infrared (IR) optics applications.[1–5] ChG-based waveguides, resonators, and interferometers have been demonstrated for photonic integrated circuits, fibers, and sensors.[6–9] In particular, the significant phase transition of ChG between the amorphous and crystalline states has enabled programmable devices for tunable photonics and optical data storage.[9] Taking the advantages of the strong interaction of light with ChG nanostructures, ChG-based devices with high compactness have been demonstrated for nonlinear optics and IR imaging.[10,11] In addition to their supreme optical properties, ChG materials have also been exploited as an inorganic photoresist in photolithography. When exposed to ultraviolet (UV) light, ChG films can be selectively photodoped with silver (Ag),[12] leading to a dramatic decrease in the solubility of the Ag-doped ChG in an ammonia-based developer compared to the undoped ChG one. The ChG-based inorganic photoresists are found superior over the organic ones in terms of both the etch selectivity and spatial resolution,[13] as evidenced by the recent development of various high-resolution and high-aspect-ratio ChG patterns.[14] However, current practices for patterning ChG films still require electron-beam lithography to dope Ag into ChG with low throughput and high cost, thus hindering the attempt to explore new ChG-based nanostructures and devices.[15]

Imprint lithography has been developed to form large-scale nanostructures, where a stamp or template with pre-defined patterns is molded into a thermal- or light-sensitive imprint resists over a substrate; and after the patterns are transferred from the template into imprint resist, the template is removed.[16–18] Because of their relatively low glass transition temperature, bulk ChG glasses can be easily molded using a stamp at an elevated temperature.[19–24] In addition, the ChG thin films can also be directly patterned using the thermal nanoimprint lithography with a critical dimension as small as 20 nm.[25–28] Although the thermal nanoimprint of ChG glasses has been successful, the patterned ChG film cannot serve as an inorganic resist to transfer patterns into its substrate due to the residual ChG materials remained at the bottom of the intended areas. It is also desirable to carry out the imprint at room temperature to avoid thermal expansions and the mismatch of thermal expansion coefficients between the stamp and ChG film.

Here, we present a new low-cost, large-scale nanofabrication approach that leverages the advantages of both the imprint lithography and silver doping (IL-SD) to form subwavelength patterns in ChG films. The IL-SD method requires an imprint stamp coated with a thin Ag layer and a UV light source with a wavelength below 500 nm, while realizing high-resolution,

L. Wei, J. Qian, Prof. L. Dong
Department of Electrical and Computer Engineering
Iowa State University
2115 Coover Hall, Ames, IA 50011, USA
E-mail: ldong@iastate.edu
Prof. M. Lu
Department of Electrical and Computer Engineering
Department of Mechanical Engineering
Iowa State University
2128 Coover Hall, Ames, IA 50011, USA
E-mail: menglu@iastate.edu
The ORCID identification number(s) for the author(s) of this article can be found under https://doi.org/10.1002/smll.202000472.

DOI: 10.1002/smll.202000472

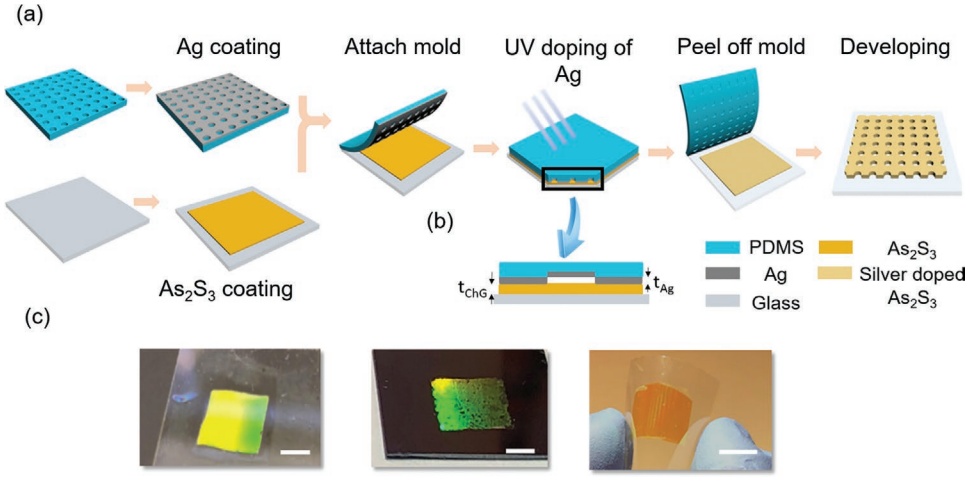

Figure 1. IL-SD fabrication process. a) Schematic process flow of using an Ag-coated PDMS stamp to generate patterns in an As_2S_3 film. b) Illustration showing the photodoping of Ag through the interface between the As_2S_3 film and the Ag-coated PDMS stamp into the As_2S_3 film. c) Photograph of the fabricated ChG nanostructures on glass (left), silicon (center), and plastic (right) substrates, respectively. Scale bars represent 1 cm.

residue-free nanostructures in ChG films with the patterning resolution smaller than the diffraction limit. The IL-SD method holds great potential for mass production of ChG-based structures and devices, as demonstrated by the realization of versatile near- and mid-IR photonic crystals (PhCs) on different substrates.

2. Results and Discussion

2.1. IL-SD Patterning of ChG Film

The IL-SD process is summarized in **Figure 1**. The method is based on the photodoping or photo-dissolution of Ag into ChG and uses an Ag-coated elastomer stamp to selectively dope Ag into a ChG film. The patterns formed in the ChG film have the same resolution as those on the stamp. While the photodoping of Ag has been reported to modify various ChG materials such as GeS_3, As_2S_3, and GeSbTe,[29,30] the As_2S_3 film was chosen to demonstrate the IL-SD process. Essentially, when illuminated by UV light with the photon energy greater than the bandgap of As_2S_3 (E_g = 2.7 eV), the As_2S_3 film absorbs the light, generating electron-hole pairs. In the presence of holes, Ag atoms are oxidized into Ag ions that can diffuse into the As_2S_3 film, driven by the build-in electrostatic field.[31] The resulting Ag-doped As_2S_3 can dissolve in an alkaline developer much slower than the undoped one.[32]

The details of the IL-SD process are described in the Experimental Section. In brief, a polydimethylsiloxane (PDMS) stamp with the desired patterns was coated with a thin Ag layer. The As_2S_3 film was deposited on a rigid or plastic substrate. Then, the PDMS stamp was brought in contact with the As_2S_3 film (Figure 1a). The UV radiation passed through the stamp and doped the Ag atoms into the As_2S_3 film. After the exposure, the As_2S_3 film was immersed in an alkaline developer to remove the undoped As_2S_3. As a result, the patterns on the stamp were transferred into the As_2S_3 film, and there was no As_2S_3 residue remaining in the patterned area. The patterning resolution of the IL-SD method is mainly determined by the original pattern on the PDMS stamp and the photodoping process. It should be noted that the spatial distribution of the Ag ions along both the vertical and lateral directions can be fine-tuned by controlling the dose of UV exposure.

The IL-SD method was successfully demonstrated to fabricate patterns with the critical dimension on the order of tens of nanometers. **Figure 2**a,b shows the scanning electron microscopy (SEM) images of the fabricated 1D gratings in As_2S_3 thin films. Figure 2a shows the 100 nm-thick As_2S_3 gratings with a period of 179 nm and the minimum feature size of 90 nm. Figure 2b presents the As_2S_3 grating with the period and duty cycle of 550 nm and 50%, respectively. The SEM images in Figure 2c–e display the 2D As_2S_3 gratings fabricated using the IL-SD process. Figure 2c shows the 2D grating with the period and hole diameter of Λ_{2D} = 300 nm and d = 150 nm, respectively. Figure 2d shows the top-view and side-view photographs of an array of nanohole with a period of Λ_{2D} = 700 nm and the As_2S_3 film thickness of t = 100 nm. In addition, the IL-SD method is also used to fabricate microscale patterns, as shown in Figure 2e, where the 2D As_2S_3 gratings have a period of Λ_{2D} = 3 µm and the hole diameter of d = 800 nm. The IL-SD process produced positive images on the ChG film with regard to the PDMS mold. By optimizing the exposure and development conditions, the imprinted pattern in As_2S_3 film can well replicate the corresponding PDMS pattern, as shown in Figure S1, Supporting Information. The element compositions of the undoped and Ag-doped As_2S_3 films were characterized using energy-dispersive X-ray spectroscopy (EDS) analysis. The EDS spectra in Figure S2, Supporting Information, show that the atomic ratios for the evaporated As_2S_3 film and Ag-doped As_2S_3 film are As/S = 1:1.41 and Ag/As/S = 1:1.83:2.52, respectively. To study how the Ag doping process can affect the optical constants, the refractive index (n) and extinction coefficient (k) of doped and undoped As_2S_3 films were measured using an ellipsometer and shown in Figure S3, Supporting Information. The doping of Ag increased the refractive index of the

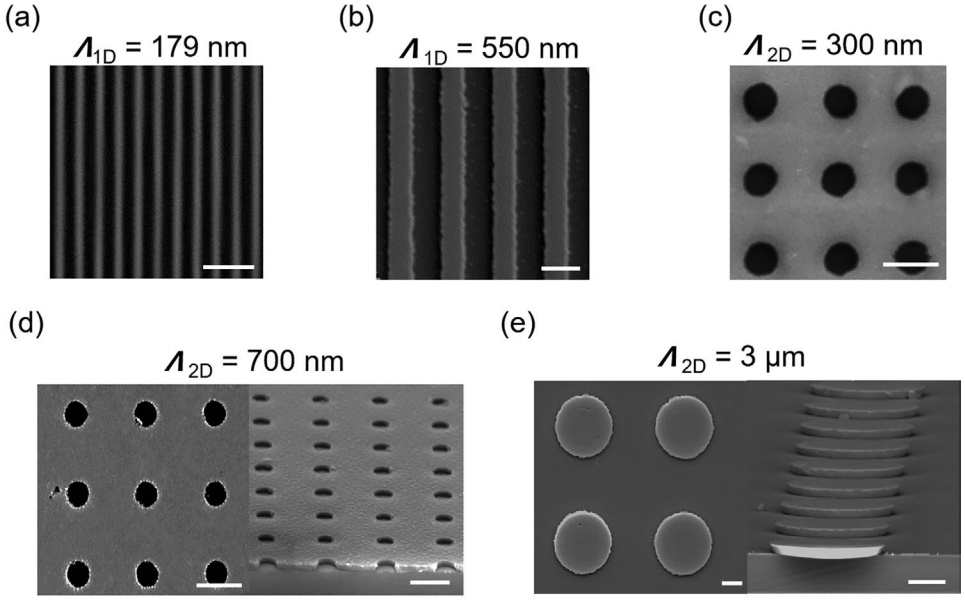

Figure 2. SEM images of the fabricated 1D and 2D ChG gratings. a) 1D ChG grating with the grating period and line width of 179 and 90 nm, respectively. b) 1D ChG grating with the grating period and line width of 550 and 275 nm, respectively. c) 2D array of nanoholes with a period of 300 nm and a hole diameter of 150 nm. d) Top view (left) and a cross-sectional view (right) of a 2D nanoholes array with the period and hole diameter of 700 and 300 nm, respectively. e) Top view (left) and a cross-sectional view (right) of the 2D array of micro discs. The array period and disc diameters are 3 and 1.5 μm, respectively. Scale bars: 500 nm.

ChG film, but the extinction coefficients remained negligible in the near-IR wavelength range.

2.2. Pattern Transferring from IL-SD-Formed ChG Film to the Substrate

For most existing nanoimprint lithography methods, after the imprint process, there remains a well-known residue layer of imprint resist in the patterned area on the substrate.[18] Before the patterns in the imprint resist can be transferred into the substrate through etching, additional efforts are needed to remove the residue layer; however, the residue layer is often so nonuniform across the substrate that complete removal of the residue layer is challenging in term of time control and etching selectivity. In contrast, the IL-SD method provides the ChG film-based etching mask that is free of the residue layer, and the substrate under the ChG mask can be etched immediately after the development step.

Here, as a demonstration, the patterned As_2S_3 film shown in Figure 2d was used as the etching mask to transfer the 2D array pattern into the thermal oxide (SiO_2) layer on a silicon wafer. The oxide layer was etched using a 10:1 buffered oxide etchant (BOE) solution for 30 s. The As_2S_3 film has a high resistance to the BOE solution. **Figure 3**a,b shows the prospective and side-view SEM images of the etched sample before the As_2S_3 etching mask was removed. Because of the isotropic BOE etch of SiO_2, the transferred nanoholes in the oxide layer exhibit lateral undercut, leading to the 300 nm hole diameter, compared to the 200 nm hole diameter of the As_2S_3 mask. The As_2S_3 layer was then stripped using ammonia hydroxide for 3 min. Figure 3c is the SEM image of the 2D array of nanoholes in SiO_2 after the removal of the As_2S_3 layer. Therefore, the IL-SD patterned ChG film can serve as an etching mask to pattern the underlying substrate by choosing an appropriate etchant solution that has a high selectivity to the substrate compared to the ChG mask. Interestingly, the patterned film of As_2S_3 can be peeled entirely from the substrate with sufficient undercuts of the oxide, as shown in Figure 3d.

2.3. ChG-Based PhCs Fabricated Using IL-SD

2.3.1. Near-IR Planar PhC

To date, PhC devices, such as PhC waveguides, cavities, and filters, have been successfully demonstrated using undoped ChG materials.[33–37] This section shows that the Ag-doped As_2S_3 PhCs can be formed using the IL-SD method and can support optical resonances, such as Fano resonance, over a broad wavelength range. The guided-mode Fano resonances have been previously reported using PhC slab structures with narrowband reflection or transmission signatures.[38] The subwavelength PhC structure can couple light at a particular wavelength and angle of incidence to a leaky guided mode supported by the grating waveguide. The interference of the guided mode and a Fabry–Pérot mode supported by the PhC thin film results in the reflection with an asymmetric Fano lineshape.[39] The underlying principle of the Fano resonance associated with the PhC structure was explained in detail by Liu et al.[40] To design the ChG-based PhC structure for a desired Fano resonance feature, the rigorous coupled-wave analysis (RCWA) was used to model light transmission through 2D ChG gratings. Based on the RCWA simulation result, the 2D grating pattern with the

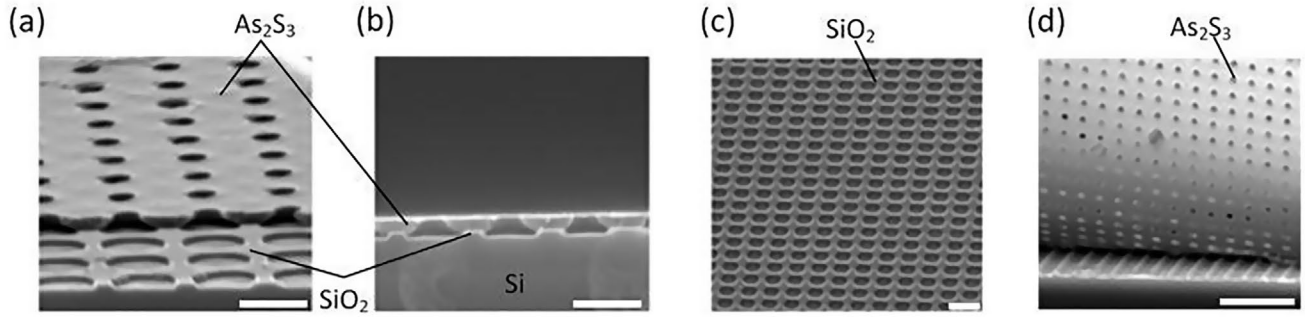

Figure 3. SEM images of using a ChG-based mask to transfer patterns from the ChG film to the substrate beneath it. a) Prospective and b) cross-sectional view of the ChG-SiO_2-Si structure after a 10 s over-etching. c) Top view of the SiO_2 pattern after removal of ChG. Scale bars represent 500 nm in (a–c) and 3 µm in (d).

period $\Lambda_{2D} = 700$ nm, depth $t = 100$ nm, and duty cycle $\eta = 50\%$ was chosen to obtain Fano resonances in the near-IR wavelength range.

The transmission characteristics of the fabricated PhCs were characterized using the optical setup shown in **Figure 4**a. Figure 4b compares the measured and simulated transmission spectra $T(\lambda)$ under the normal incidence of light ($\theta_i = 0°$). The resonance feature in the transmittance was found to follow the asymmetric Fano lineshape. The measured spectrum was fitted using a Lorentzian function, based on which the Fano parameter of $q = 1$ and the resonance wavelength of $\lambda_r = 1100$ nm were obtained. The optical resonance implies an enhanced and confined local field around the PhC slab. Figure 4c shows the spatial distribution of the simulated electric field at the cross section of the PhC slab. The resonance phenomenon at $\lambda_r = 1100$ nm can result in nearly one order magnitude higher electric field compared to the incidence. The resonance signatures vary with the changing angle of incidence. The photonic band diagram of the PhC was obtained by measuring its transmittance as a function of incidence angle θ_i. Figure 4d shows the measured band diagram with the incidence angle from $\theta_i = 0°$ to 10° over the wavelength range from $\lambda = 900$ to 1300 nm.

2.3.2. Mid-IR Flexible PhC

In addition to high mechanical flexibility, another attractive feature of the materials is their low material loss in the mid-IR wavelength range. The IL-SD method can be exploited to form mid-IR flexible PhCs inexpensively. As an example, the periodic microstructure was fabricated on a 180 µm-thick flexible acetate substrate that is transparent in the mid-IR wavelength range from 4 to 5 µm. Fourier transform infrared (FTIR) spectrometry

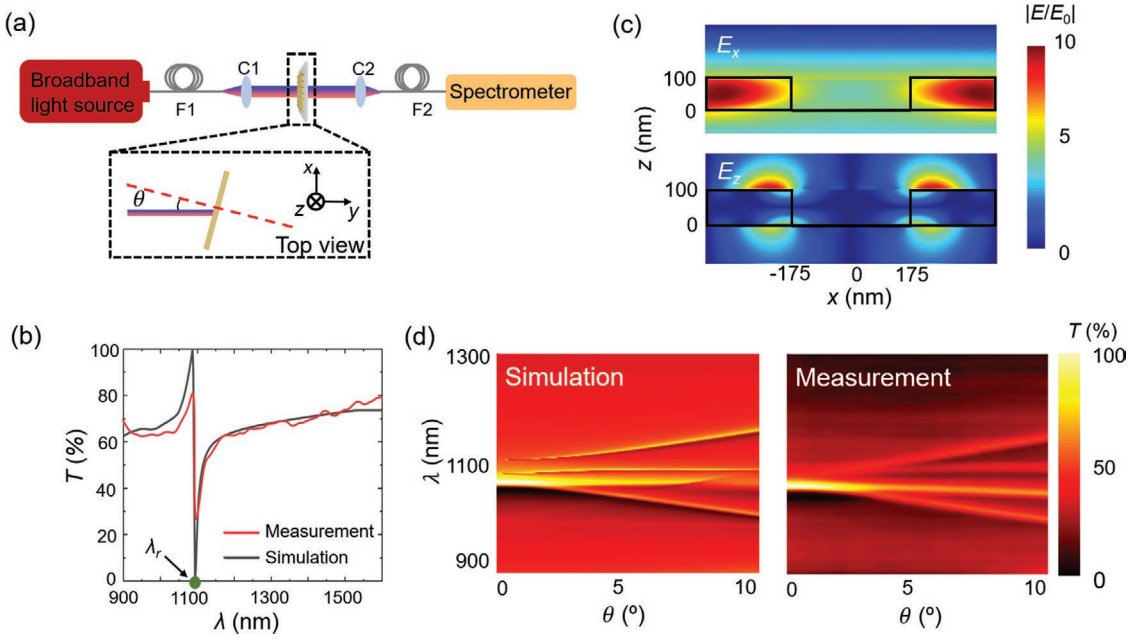

Figure 4. Optical characterization of the Ag-doped As_2S_3 PhC slab. a) Schematic of the near-IR transmission measurement setup, where F1 and F2 represent multimode optical fibers, and C1 and C2 are the collimation lens. b) Simulated and measured transmission spectra of the ChG-based PhC with $\Lambda_{2D} = 700$ nm. c) Calculated near-field distributions within one period of the 2D grating at $\lambda_r = 1100$ nm. The E_x and E_z profiles are shown by the top and bottom plots, respectively. d) Simulated and measured transmittance as a function of incidence angle.

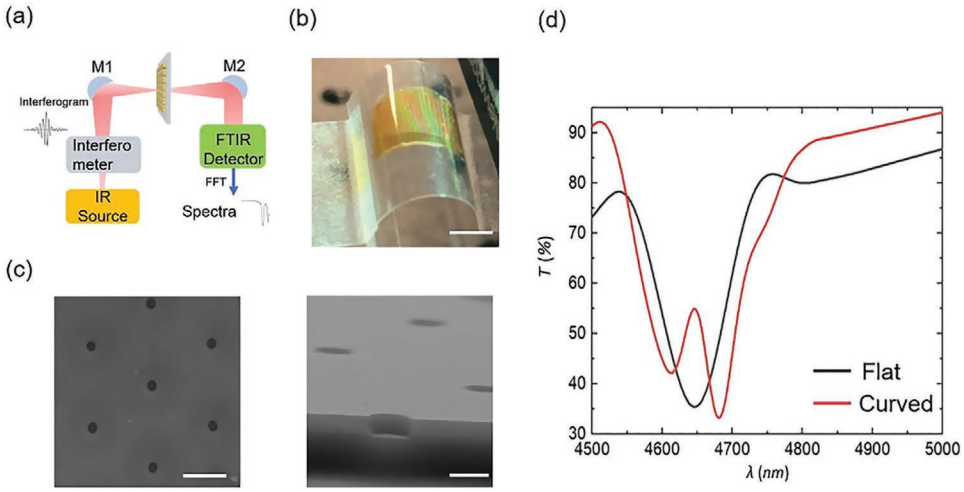

Figure 5. Characterization of the mid-IR flexible ChG PhC. a) Schematic of the mid-IR transmission measurement setup using an FTIR spectrometer. b) Photography of the ChG PhC on a plastic substrate that is bent to the radius of curvature of 35 mm. c) Top view (left) and a cross-sectional view (right) of the mid-IR ChG PhC that has the period, hole diameter, and film thickness of 3 µm, 500 nm, and 300 nm, respectively. d) Measured transmission spectra of the ChG PhC before and after being bent.

(**Figure 5**a) was used to characterize the transmittance of the mid-IR PhC slab formed on the acetate substrate (Figure 5b). The SEM images in (Figure 5c) show the top and cross-sectional views of the PhC with the period of Λ_{2D} = 3 µm and the hole diameter of 800 nm fabricated on the acetate substrate. When the angle of incidence was set to 0°, the PhC resonance appeared in mid-IR with the resonance peak at 4650 nm as shown by the black curve in Figure 5d. The flexible ChG PhC can be bent to obtain a 35 mm-radius curvature (Figure 5b). Due to the bending, the incident angle increased with regard to the sample surface. The off-normal incidence resulted in two resonances, which were split from the 4650 nm resonance for the normal incidence case. The shift of Fano resonances as a function of incidence angle agrees with the photonic band diagram shown in Figure 4d.

2.4. Tuning the Optical Resonance of PhC through Size Control

Further, the IL-SD method can enable a flexible method to control the final size of the patterns formed in the ChG film, even though the PDMS stamp contains fixed patterns. The rationale is that the spatial distribution of Ag in the ChG film can be precisely controlled during the doping. The controlled Ag atoms diffusions along both vertical and lateral directions allow us to manage the distribution of Ag in the ChG film, thus tune the final size of the ChG patterns after the development.

As a demonstration, the IL-SD process was applied to transfer the 700 nm-period 2D grating pattern into a 100 nm-thick As_2S_3 film at four different UV exposure doses. Under the UV power density of 80 µW mm^{-2}, the vertical Ag doping in the As_2S_3 film completed after ≈200 s, which corresponded to a vertical Ag diffusion rate of 0.5 nm s^{-1}. Afterward, if the UV exposure continues, the Ag ions mainly diffuse in the lateral direction as illustrated in **Figure 6**a. As a result, excessive UV exposure can be exploited to fine-tune the grating duty cycle. Figure 6b shows the SEM images of the As_2S_3 PhCs fabricated with four different UV doses at 24, 36, 48, and 60 mJ mm^{-2}. The increase of the UV dose results in reducing the nanohole diameter from 300 to 50 nm. Based on the change of the hole diameter, the lateral diffusion rate of 0.2 nm s^{-1} was calculated. The transmission spectra of the four nanohole arrays with the hole diameters of 50, 180, 210, and 300 nm are plotted in Figure 6c,d. Both the RCWA simulation and measurement results show that the Fano resonance characteristics of the PhC slabs can be tuned with the final diameter of the nanohole. With increasing hole diameter, the effective refractive index of the PhC slab increases, and consequently, the resonance wavelength shifted towards a longer wavelength. Also, as the hole diameter was shrunk, the coupling efficiency between the Fano resonance mode and free space propagation mode reduced. As a result, the As_2S_3 PhC with a smaller nanohole exhibited a sharper resonance and the corresponding quality factor increases from 54.5 to 524.4. It is worth noting that the resonance feature of the PhC structure can be affected by other geometric and material properties, such as the grating period, ChG thickness, and substrate material. However, these properties are usually set during the design stage and cannot be changed during a lithography or imprint process. In contrast, the IL-SD method makes it possible to tune the PhC resonance.

3. Conclusion

This article reports a new nanolithography approach that integrates the UV light-controlled Ag doping method with the imprint lithography to pattern ChG films. The approach uses the Ag-coated PDMS stamp to selectively transfer Ag into the ChG film during UV exposure. The undoped ChG region can be subsequently removed via wet etching. Using the approach, we have fabricated various1D and 2D gratings in As_2S_3 film with the feature size as small as 50 nm, and have demonstrated that the patterned As_2S_3film can be used as an etching mask to transfer the nanohole arrays from the patterned to the oxide

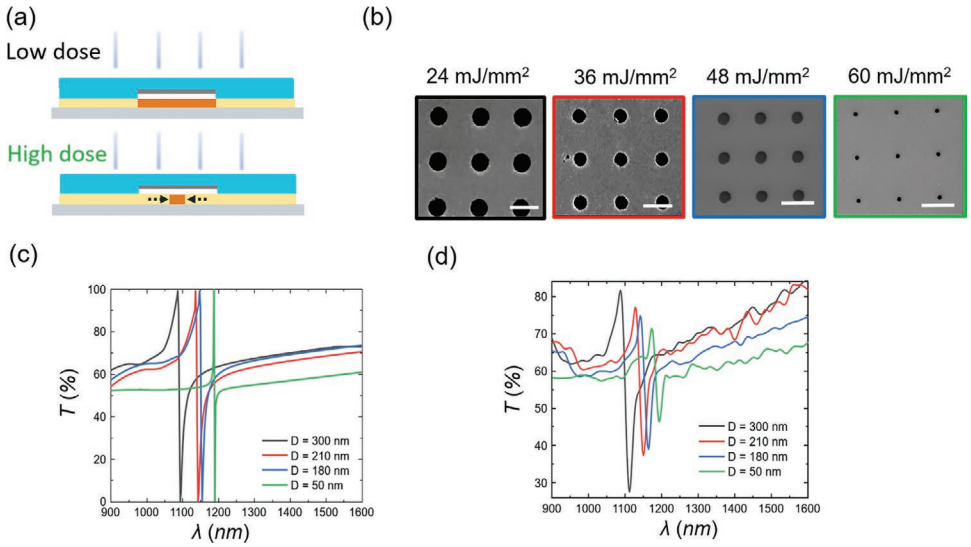

Figure 6. Tuning the pattern size and the optical resonance of the As_2S_3 PhC via controlled lateral diffusion of Ag. a) Schematic of the lateral diffusion during the photodoping of Ag. b) SEM images of 2D nanohole arrays with the hole diameter ranging from 300 to 50 nm. These patterns are formed based on a single PDMS stamp. Scale bars represent 500 nm. c) Simulated and d) measured transmission spectra of the obtained 2D nanohole arrays shown in (b).

substrate using wet etching. There was no residue layer found in the patterned region on the substrate and it is possible to transfer the patterns into the substrate without an additional etching process. Because ChG is generally stable in fluorine plasma, the patterned ChG film is useful as an etching mask for dry etching the substrate material underneath the ChG. We have successfully employed the IL-SD method to develop As_2S_3-based planar near-IR and flexible mid-IR PhC slabs that exhibit strong Fano resonances. Furthermore, we demonstrated the ability of the IL-SD process to modulate the spatial distribution of Ag inside the ChG film, thus tune the final size of the patterns in the ChG film, without using different PDMS stamps.

Besides the new ability to produce nanostructures in ChG materials with low cost and high throughput over a large area, the IL-SD approach represents a simple but effective residue-free solution to nanoimprint lithography. This method provides not only a 50 nm minimum feature size in the As_2S_3 film but also surpasses many conventional nanoimprint lithography techniques that leave a residue layer in the resist after imprinting a UV-sensitive polymer or hot embossing thermoplastic polymer. Consequently, the formed As_2S_3 patterns can be transferred into the supporting substrate without any additional etch-back process.

We envision that the IL-SD approach could also be adopted by the existing nanoimprint lithography tools, such as Canon's S-FIL and EVG's SmartNIL systems, by simply coating a thin Ag layer on a template and using a ChG film as the solid-state imprint resist.[41,42] The use of a dedicated nanoimprint tool can benefit the contact between the PDMS stamp and ChG samples by reducing trapped air bubbles and other defects. We note that the IL-SD approach has room for further improvement. For example, the lateral diffusion of Ag ions needs to be a better controller to enhance the pattern anisotropy. Also, while the PDMS stamp can be reused, there is a need to deposit Ag again on the surface of the stamp, which will increase the fabrication cost. The future work will be focused on testing various potential mold materials to realize selective Ag doping of ChG films with high aspect ratios and exploring various ChG-based IR optics for their applications in biochemical sensing and optical communication.

4. Experimental Section

IL-SD Fabrication Process: The PDMS stamps used in this work were produced by replicating silicon master wafers that carry the negative profiles of the desired patterns. The silicon master wafers were fabricated using electron-beam lithography or UV lithography followed by reactive ion etching. The 10 nm-thick Ag layer was deposited on the PDMS stamp using an electron beam evaporator (BJD-1800, Temescal). The As_2S_3 films were evaporated on the glass and plastic substrates using the same evaporator. The thickness, refractive index, and extinction coefficient of the coated As_2S_3 film were measured using an ellipsometer (alpha-SE, J.A. Woollam Co.). During the IL-SD process, the PDMS stamp was carefully attached to and held against the ChG film by its own gravity. To dope Ag, the PDMS-covered As_2S_3 sample was illuminated under the 365 nm UV light (P = 40 W, Dymax). When the target exposure dose was reached, the PDMS stamp was removed and the doped As_2S_3 sample was dipped in a developer (MIF-300, Integrated Micro Materials). The development time was controlled to dissolve the undoped region while keeping the Ag-doped region.

Electromagnetic Simulation: The RCWA simulations were performed using a commercial modeling tool (DiffractMOD, Synopsys). The simulation domain included only one period of the 2D ChG structures with the periodic boundary conditions to truncate the 2D grating at the x-axis and y-axis (Figure 4a). The refractive index ($n(\lambda)$) and extinction coefficient ($k(\lambda)$) of As_2S_3 film were interpolated using the results obtained from the ellipsometry measurement. The incidence of plane-wave was linearly polarized along the x-axis. The transmission spectra were calculated in the wavelength range of 900–1600 nm. At the resonance wavelength, the electric field (E_x and E_z) distributions in the simulation domain were calculated.

Near- and Mid-IR Transmission Measurements: The near-IR transmission measurements were carried out using a home-built

setup. The setup used a fiber-coupled broadband light source (Luxtec Fiberoptics) as the excitation. The excitation light was collimated using a fiber tip collimator (F240SMA, Thorlabs). The ChG PhC sample under test was mounted on a rotation stage. The transmitted light was coupled into a collection fiber and analyzed using a near-IR spectrometer (EPP 2000, StellarNet). The reference spectrum was taken by measuring the transmission of an un-patterned As_2S_3 sample. The reference spectrum was used to calculate the transmission coefficients. To investigate how the transmittance changed versus θ_i, the sample transmission spectra were recorded when the angle of incidence was tuned from 0° to 10° with the increment of 0.5°. The photonic band diagram was generated by plotting the sample transmission as a function of θ_i using MATLAB. The mid-IR transmission was characterized using an FTIR spectrometer (FTS 7000 DigiLab).

Supporting Information

Supporting Information is available from the Wiley Online Library or from the author.

Acknowledgements

This research was supported by the National Science Foundation through the grant numbers ECCS-1711839 and ECCS-1653673. Any opinions, findings, and conclusions or recommendations expressed in this material are solely the responsibility of the authors and do not necessarily represent the official views of the National Science Foundation.

Conflict of Interest

The authors declare no conflict of interest.

Keywords

chalcogenides, imprint lithography, infrared optics, photonic crystals

Received: January 23, 2020
Revised: March 1, 2020
Published online: April 20, 2020

[1] D. Lezal, J. Pedlikova, J. Zavadil, *J. Optoelectron. Adv. Mater.* **2004**, *6*, 133.
[2] A. Faraon, D. Englund, D. Bulla, B. Luther-Davies, B. J. Eggleton, N. Stoltz, P. Petroff, J. Vučković, *Appl. Phys. Lett.* **2008**, *92*, 043123.
[3] B. J. Eggleton, B. Luther-Davies, K. Richardson, *Nat. Photonics* **2011**, *5*, 141.
[4] H. T. Lin, Y. Song, Y. Z. Huang, D. Kita, K. Q. Wang, L. Li, J. Y. Li, H. Y. Zheng, Z. Q. Luo, S. Novak, C. C. Huang, D. Hewak, K. Richardson, J. Kong, J. J. Hu, *Conf. Lasers Electro-Opt. Eur.* **2017**, p. 798.
[5] J. L. Adam, L. Calvez, J. Troles, V. Nazabal, *Int. J. Appl. Glass Sci.* **2015**, *6*, 287.
[6] N. P. Eisenberg, M. Manevich, M. Klebanov, V. Lyubin, S. Shtutina, *J. Non-Cryst. Solids* **1996**, *198–200*, 766.
[7] Z. Q. Tang, V. S. Shiryaev, D. Furniss, L. Sojka, S. Sujecki, T. M. Benson, A. B. Seddon, M. F. Churbanov, *Opt. Mater. Express* **2015**, *5*, 1722.
[8] T. Kleine, R. Glass, R. Norwood, J. Pyun, *Abstr. Pap. Am. Chem. Soc.* **2019**, *37*, 141.
[9] L. J. Liu, H. A. Khan, J. J. Li, A. C. Hillier, M. Lu, *Nanotechnology* **2016**, 27, 295301.
[10] C. R. Petersen, N. Prtljaga, M. Farries, J. Ward, B. Napier, G. R. Lloyd, J. Nallala, N. Stone, O. Bang, *Opt. Lett.* **2018**, *43*, 999.
[11] G. Lenz, J. Zimmermann, T. Katsufuji, M. E. Lines, H. Y. Hwang, S. Spalter, R. E. Slusher, S. W. Cheong, J. S. Sanghera, I. D. Aggarwal, *Opt. Lett.* **2000**, *25*, 254.
[12] A. Lorinczi, M. Popescu, F. Sava, A. Velea, I. D. Simandan, *Phys. Status Solidi C* **2011**, *8*, 2617.
[13] A. Kovalskiy, J. Cech, M. Vlcek, C. M. Waits, M. Dubey, W. R. Heffner, H. Jain, *J. Micro/Nanolithogr., MEMS, MOEMS* **2009**, *8*, 043012.
[14] G. C. Chern, I. Lauks, *J. Appl. Phys.* **1982**, *53*, 6979.
[15] R. Elghrandi, J. Calas, G. Galibert, M. Averous, *Thin Solid Films* **1992**, *218*, 259.
[16] S. H. Ahn, L. J. Guo, *ACS Nano* **2009**, *3*, 2304.
[17] S. Y. Chou, P. R. Krauss, W. Zhang, L. Guo, L. Zhuang, *J. Vac. Sci. Technol. B* **1997**, *15*, 2897.
[18] S. Y. Chou, P. R. Krauss, P. J. Renstrom, *J. Vac. Sci. Technol., B: Microelectron. Nanometer Struct.—Process., Meas., Phenom.* **1996**, *14*, 4129.
[19] C. R. Petersen, M. B. Lotz, G. Woyessa, A. N. Ghosh, T. Sylvestre, L. Brilland, J. Troles, M. H. Jakobsen, R. Taboryski, O. Bang, *Opt. Lett.* **2019**, *44*, 5505.
[20] A. Pandey, S. Tzadka, D. Yehuda, M. Schvartzman, *Soft Matter* **2019**, *15*, 2897.
[21] M. R. Lotz, C. R. Petersen, C. Markos, O. Bang, M. H. Jakobsen, R. Taboryski, *Optica* **2018**, *5*, 557.
[22] D. Yehuda, E. Kassis, S. Joseph, M. Schvartzman, *J. Vac. Sci. Technol., B* **2018**, *36*, 031602.
[23] N. Ostrovsky, D. Yehuda, S. Tzadka, E. Kassis, S. Joseph, M. Schvartzman, *Adv. Opt. Mater.* **2019**, *7*, 1900652.
[24] J. Orava, T. Kohoutek, A. L. Greer, H. Fudouzi, *Opt. Mater. Express* **2011**, *1*, 796.
[25] M. Solmaz, H. Park, C. K. Madsen, X. Cheng, *J. Vac. Sci. Technol., B: Microelectron. Nanometer Struct.—Process., Meas., Phenom.* **2008**, *26*, 606.
[26] S. Danto, E. Koontz, Y. Zou, T. O. Ogbuu, B. Gleason, P. Wachtel, J. D. Musgraves, J. J. Hu, K. Richardson, *Proc. SPIE* **2013**, *8884*, 88841T.
[27] Y. Zou, D. N. Zhang, H. T. Lin, L. Li, L. Moreel, J. Zhou, Q. Y. Du, O. Ogbuu, S. Danto, J. D. Musgraves, K. Richardson, K. D. Dobson, R. Birkmire, J. J. Hu, *Adv. Opt. Mater.* **2014**, *2*, 478.
[28] T. Han, S. Madden, D. Bulla, B. Luther-Davies, *Opt. Express* **2010**, *18*, 19286.
[29] P. Singh, A. P. Singh, J. Sharma, A. Kumar, M. Mishra, G. Gupta, A. Thakur, *Phys. Rev. Appl.* **2018**, *10*, 054070.
[30] M. Mitkova, M. N. Kozicki, *J. Phys. Chem. Solids* **2007**, *68*, 866.
[31] P. Khan, Y. S. Xu, W. Leon, K. V. Adarsh, D. Vezenov, I. Biaggio, H. Jain, *J. Non-Cryst. Solids* **2018**, *500*, 468.
[32] B. Singh, S. P. Beaumont, P. G. Bower, C. D. W. Wilkinson, *Appl. Phys. Lett.* **1982**, *41*, 889.
[33] M. W. Lee, C. Grillet, C. L. C. Smith, S. Tomijenovic-Hanic, D. J. Moss, B. J. Eggleton, D. Freeman, B. Luther-Davies, S. Madden, A. Rode, Y. Ruan, Y. H. Lee, *Opt. Express* **2007**, *15*, 1277.
[34] J. Fatome, C. Fortier, T. N. Nguyen, T. Chartier, F. Smektala, K. Messaad, B. Kibler, S. Pitois, G. Gadret, C. Finot, J. Troles, F. Desevedavy, P. Houizot, G. Renversez, L. Brilland, N. Traynor, *J. Lightwave Technol.* **2009**, *27*, 1707.
[35] C. Grillet, D. Freeman, B. Luther-Davies, S. Madden, R. McPhedran, D. J. Moss, M. J. Steel, B. J. Eggleton, *Opt. Express* **2006**, *14*, 369.
[36] A. Faraon, D. Englund, D. Bulla, B. Luther-Davies, B. J. Eggleton, N. Stoltz, P. Petroff, J. Vuckovic, *Appl. Phys. Lett.* **2008**, *92*, 043123.
[37] Y. L. Ruan, M. K. Kim, Y. H. Lee, B. Luther-Davies, A. Rode, *Appl. Phys. Lett.* **2007**, *90*, 071102.
[38] A. E. Miroshnichenko, S. Flach, Y. S. Kivshar, *Rev. Mod. Phys.* **2010**, *82*, 2257.

[39] *Photonic Crystal Metasurface Optoelectronics*, 1st ed. (Eds: W. D. Zhou, S. H. Fan), Academic Press, San Diego, CA **2019**.
[40] J. N. Liu, M. V. Schulmerich, R. Bhargava, B. T. Cunningham, *Opt. Express* **2014**, *22*, 18142.
[41] F. Delachat, J. C. Phillipe, V. Larrey, F. Fournel, S. Bos, H. Teyssedre, X. Chevalier, C. Nicolet, C. Navarro, I. Cayrefourcq, *Proc. SPIE* **2018**, *10586*, 1058615.
[42] S. V. Sreenivasan, C. G. Willson, N. E. Schumaker, D. J. Resnick, *Proc. SPIE* **2002**, *4608*, 8.